

# The JHU Turbulence Databases (*JHTDB*)

## TRANSITIONAL BOUNDARY LAYER DATA SET

*Data provenance:* J. Lee & T. A. Zaki

*FileDB storage and WebServices:* Z. Wu, R. Ravoori, G. Lemson, R. Burns, A. Szalay,  
C. Meneveau & IDIES staff

Johns Hopkins University, Baltimore, MD 21218

The transitional boundary-layer dataset is produced from direct numerical simulations (DNS) of incompressible flow over a flat plate with an elliptical leading edge. While the full simulation domain is shown in figure 1(a), only data from the domain over the flat region of the upper plate is stored in the JHTDB. The coordinate system is shown in figure 1(b), where the streamwise, vertical and spanwise coordinates are denoted by  $x$ ,  $y$  and  $z$ , and corresponding velocity components are  $u$ ,  $v$  and  $w$ . The half-thickness of the plate,  $L$ , is used as a reference length-scale, and the reference velocity is the incoming free-stream speed  $U_\infty$ . The length of the plate is  $L_x = 1050L$  measured from the leading edge ( $x = 0$ ), and its width is  $L_z = 240L$ . The leading-edge geometry is a super ellipse with the stagnation point located at  $(x, y) = (0, -L)$ ,

$$\left(1 - \frac{1}{AR} \frac{x}{L}\right)^4 + \left(\frac{y+1}{L}\right)^2 = 1, \quad (1)$$

where  $AR = 20$  is the aspect ratio of the ellipse. The Reynolds number based on the plate half-thickness, free-stream speed and fluid viscosity is  $Re_L \equiv U_\infty L / \nu = 800$ . The stored data correspond to  $x \in [30.2185, 1000.065]L$ ,  $y \in [0.0036, 26.4880]L$  and  $z \in [0, 240]L$ .

### Inflow free-stream turbulence

The inflow condition at the upstream curved boundary of the domain is a superposition of a uniform velocity  $U_\infty$  and turbulent fluctuations  $\mathbf{u}'_{\text{FST}}$ . The free-stream disturbances decay as they are advected towards the leading edge, and their intensity at the start of the plate is  $Tu = 3\%$  which is similar to the T3A benchmark experiment by (Roach & Brierley, 1992). Downstream, the free-stream perturbations interact with the underlying laminar boundary layer and cause bypass transition of the boundary layer to turbulence (Zaki, 2013; Nolan & Zaki, 2013).

The inflow perturbations were obtained from a precursor, pseudo-spectral simulation of decaying homogeneous isotropic turbulence (HIT) in a periodic domain. The domain sizes were  $(L_x, L_y, L_z)_{\text{FST}} = (240, 15, 240)L$  and the corresponding number of Fourier modes were (2048, 128, 2048). A snapshot of the evolution of the turbulence was stored as used as an inflow condition, which guided the choice of the HIT domain size. In the wall-normal direction, the HIT domain can be copied without affecting accuracy since only one box will interact with the leading edge and the boundary layer. In the span, the size matched the main simulation in order to avoid unphysical spanwise correlations. Since Taylor's hypothesis transforms the streamwise spatial coordinate into time, the streamwise length of the HIT domain was long. In addition, in order to avoid a periodic inflow condition, the box of HIT was rotated around its  $z$ -axis by an angle  $\alpha$  (see figure 2). In this manner, the selected inflow plane was shifted vertically by one integral lengthscale after every

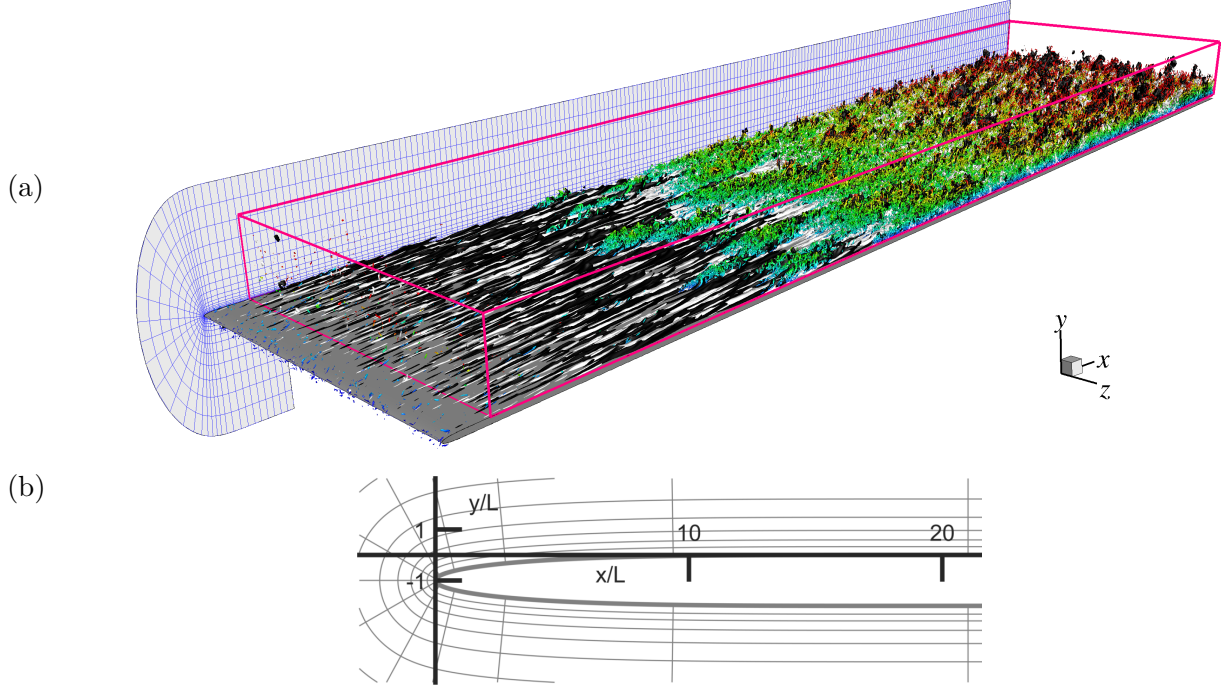


Figure 1: (a) Visualization of the computational domain for the boundary-layer simulation. (Color) Vortical structures,  $\lambda_2 = -0.01U_\infty^2/L^2$ ; streamwise velocity fluctuations, (black)  $u' = -0.1U_\infty$  and (white)  $u' = 0.1U_\infty$ ; (side view) computational grid (every sixteenth grid line is plotted). The rectangular box marks the domain stored in the JHTDB. (b) Origin of the coordinate system.

$L_{x,FST}/(U_\infty \cos \alpha)$  time units. We also ensured that the ratio of the vertical shift to the height of the inflow box,  $L_k/L_{y,FST}$ , is an irrational number.

The length-scale of the inflow turbulence is  $L_k = 1.8L$ , the Taylor Reynolds number is  $Re_\lambda = 24.2$ , and the turbulence intensity is  $Tu = 0.035$ . The energy spectrum of the stored turbulent field is shown in figure 2, where it is compared to the data by Wang *et al.* (1996). Once prescribed at the inflow to the main simulation, the free-stream turbulence intensity decays with the streamwise position according to  $(x - x_g)^{-0.8}$ . The intensity is approximately  $Tu = 3\%$  at the leading edge, and slightly less than  $Tu = 0.5\%$  at the exit of the boundary-layer simulation domain.

## Boundary-layer simulation details

Direct numerical simulation (DNS) of the boundary-layer flow over the plate was performed by discretizing the Navier-Stokes equation on a curvilinear grid (figure 1). A fractional-step algorithm was adopted, and the spatial discretization was a staggered volume-flux formulation (Rosenfeld *et al.*, 1991). The viscous terms were integrated in time implicitly using the Crank–Nicolson and the advection terms were treated explicitly using the Adams–Bashforth scheme. Pressure was treated using implicit Euler in the  $\delta p$ -form. The pressure equation was Fourier transformed in the span, and the resulting Helmholtz equation was solved for every spanwise wavenumber using two-dimensional multi-grid. The DNS code has been validated in numerous previous studies (e.g., Zaki *et al.*, 2010; Lee *et al.*, 2013, 2017).

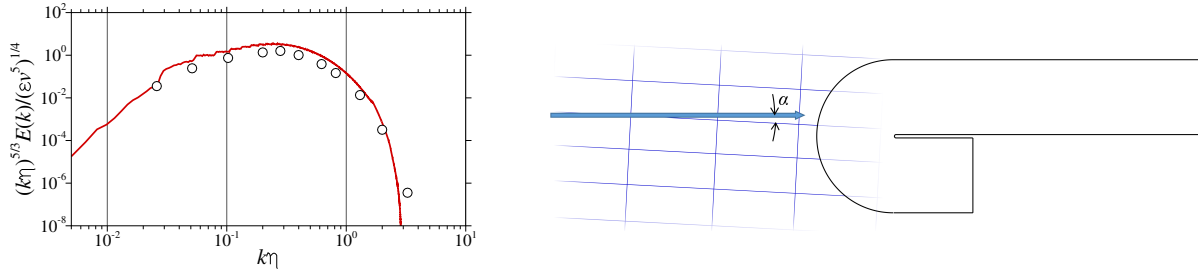


Figure 2: Left: Three-dimensional energy spectrum of inflow homogeneous isotropic turbulence in Kolmogorov scaling, at Taylor Reynolds number  $Re_\lambda = 24.2$ . Symbols are data at  $Re_\lambda = 20.9$  from Wang *et al.* (1996). Right: Schematic of inflow condition to main simulation.

| $(L_x, L_y, L_z)/L$ | $(N_x, N_y, N_z)$ | $\Delta x^+$ | $\Delta y_{min}^+$ | $\Delta z^+$ |
|---------------------|-------------------|--------------|--------------------|--------------|
| (1050, 40, 240)     | (4097, 257, 2049) | 11.9         | 0.124              | 4.07         |

Table 1: Domain size, number of grid points, and spatial resolution of boundary-layer simulation, all reported at  $x = 1000L$ .

At the wall, a no-slip boundary condition is applied, while periodic boundary conditions are applied in the spanwise direction. The boundary condition at the top of the computational domain used continuity and an active control to keep the zero pressure gradient (ZPG) in both laminar and turbulent regions. An advection boundary condition is applied at the downstream end of the top region;. The outflow boundary condition on the bottom surface is a mirror copy of the same grid line on the top surface Lee & Zaki (2018).

The domain size and grid resolution are listed in table 1. The leading-edge region ( $x < 20$ ) was discretized using 475 grid points in the wall-tangential direction, with minimum grid spacing  $0.001L$  at the leading edge (stagnation point). Far downstream ( $x = 1000$ ), the streamwise spacing is  $\Delta x^+ = 11.9$ . At the same streamwise location, the wall-normal grid spacing in the immediate vicinity of the wall is  $y_{min}^+ = 0.124$ , and 29 grid points are located within  $y^+ < 10$ . Grid stretching in both the wall-tangential and normal directions was kept at less than 3% between adjacent cells, throughout the domain. The grid spacing in the spanwise direction is  $0.117L$  uniform across the domain and, at  $\tilde{x} = 1000$ , it corresponds to  $\Delta z^+ = 4.07$ . The simulation time-step is fixed at  $\Delta t = 0.005L/U_\infty$ .

The simulation has been conducted using compute resources at the San Diego Supercomputing Center (SDSC) Comet and the Maryland Advanced Research Computing Center (MARCC). Three-dimensional flow fields were stored in two domains; the shallow body-fitted domain near the leading edge and a rectangular domain downstream — only the latter is currently part of the JHTDB. Both regions are stored in full spatial-resolution with a time-step between stored snapshots of  $\Delta t_{ins} = 0.25L/U_\infty$ . This time separation between snapshots is sufficiently small for the stored data to be considered temporally well resolved. A total of 4701 snapshots have been stored for a total time equal to  $1175.0L/U_\infty$ , about one flow through time. The total amount of data stored corresponds to about 105 Terabytes in single precision.

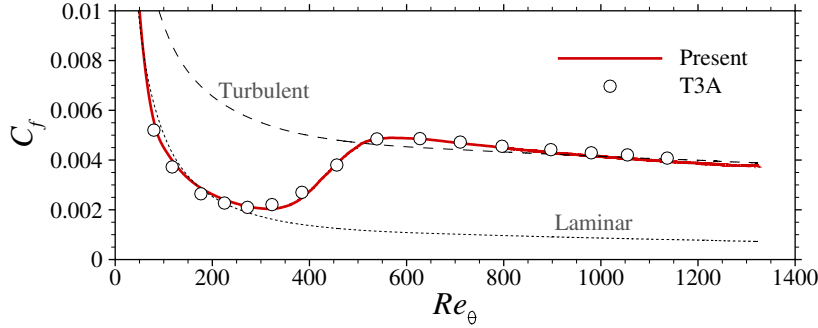


Figure 3: Skin-friction coefficient versus  $Re_\theta$ . (Dotted) Laminar level  $C_f = 0.664/\sqrt{Re_x}$ ; (dashed) turbulent correlation  $C_f = 0.445/(\log 0.06Re_x)^2$ ; (symbols) T3A data (Roach & Brierley, 1992).

### Flow statistics

The skin-friction coefficient,  $C_f$ , is plotted in figure 3 versus the momentum-thickness Reynolds number,  $Re_\theta$ . The figure shows excellent agreement with the data from the reference T3A experiment (Roach & Brierley, 1992), including the slightly lower  $C_f$  than laminar value in the upstream region at  $Re_\theta \approx 60$  due to the finite thickness of the plate. Also, the onset and end of the transition region are consistent with the experiment.

A comparison of the mean velocity and root-mean-square fluctuations from the present simulation and T3A data is provided in figure 4. Additional data at  $Re_\theta = 1000$  from the work by Schlatter *et al.* (2009) are also included in the figure. The streamwise mean velocity agrees with both previous experiments and computations. The stresses are also in agreement in the inner region of the boundary layer, but deviate from the simulation data by Schlatter *et al.* (2009) in the outer flow due to the presence of free-stream turbulence.

Contour plot of the mean velocities are shown in figure 5. A magnified view near the leading-edge stagnation point is also provided. The mean streamwise velocity (figure 5a) shows the boundary-layer development, and the marked  $u = 0.99U_\infty$  contour (dashed line) provides a measure of the boundary-layer thickness. The change in the growth rate of that contours near  $x \approx 350L$  marks the transitional region. The mean vertical velocity is shown in figure 5(b). Near the leading edge (figure 5bi), the presence of the finite-thickness body induces the abrupt change in the vertical velocity. In the transitional region, centered around  $x \approx 350L$ , the negative  $V$  is required by continuity to effect the change in the  $U(y)$  profile from laminar to turbulence since  $\partial U/\partial x > 0$  in the near-wall region. Figure 5(c) shows the streamwise gradient of the mean pressure. Owing to the top boundary condition, the pressure gradient is nearly zero in the flat-wall region, irrespective to the laminar and turbulent regions.

Figure 6 shows the variation of the Reynolds stress in the domain. Upstream of the leading edge, the three components of normal stresses are finite while the shear stress is nearly zero. The streamwise fluctuations amplify in the boundary layer, immediately downstream of the leading edge. In the transition zone, the wall-normal peak in the streamwise stress moves toward the wall. In addition, the Reynolds shear stress increases as well as the normal and spanwise normal stresses. Downstream of the transition zone, the distribution of stresses approaches, and ultimately recovers, that of a fully turbulent boundary layer.

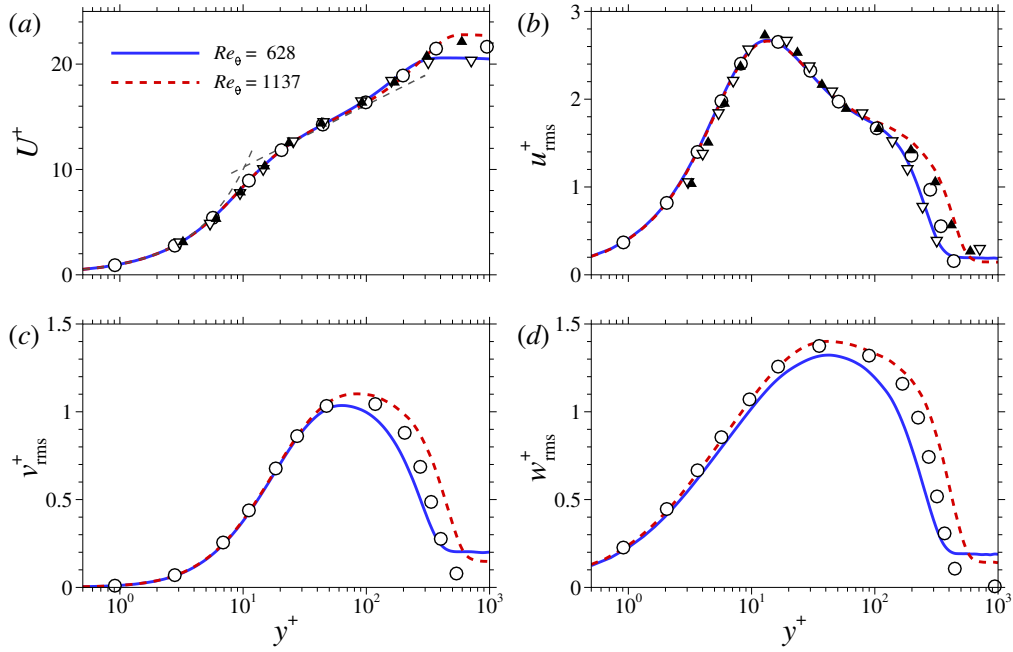


Figure 4: Turbulence statistics at  $Re_\theta = 628$  and  $1137$  normalized by the friction velocity; (a) mean streamwise velocity and r.m.s. of (b) streamwise, (c) vertical and (d) spanwise velocity fluctuations. Symbols correspond to data at ( $\nabla$ )  $Re_\theta = 628$  and ( $\blacktriangle$ )  $1137$  from the T3A experiments (Roach & Brierley, 1992); ( $\circ$ )  $Re_\theta = 1000$  by Schlatter *et al.* (2009).

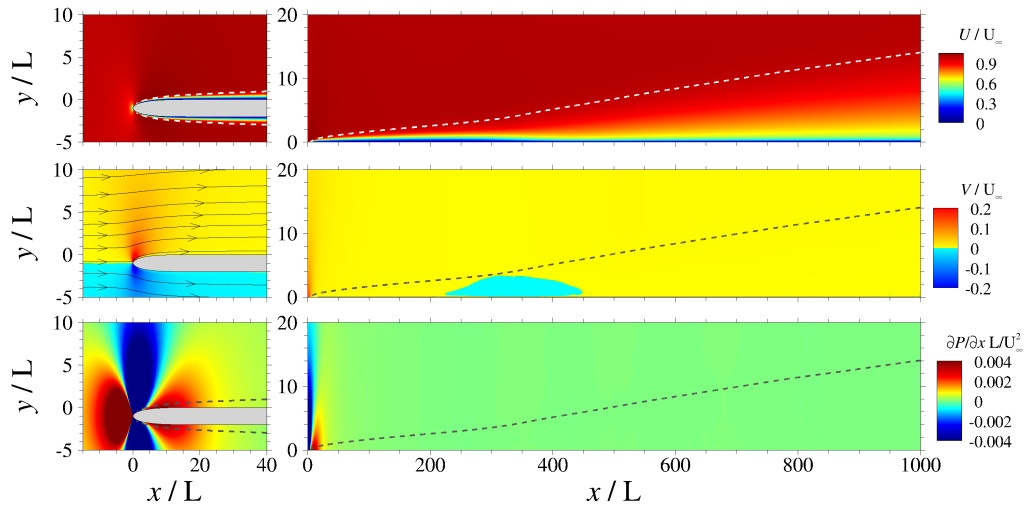


Figure 5: Time- and spanwise-averaged (top) streamwise velocity, (middle) vertical velocity and (bottom) streamwise mean-pressure gradient. The dashed line marks the iso-contour  $u = 0.99U_\infty$ .

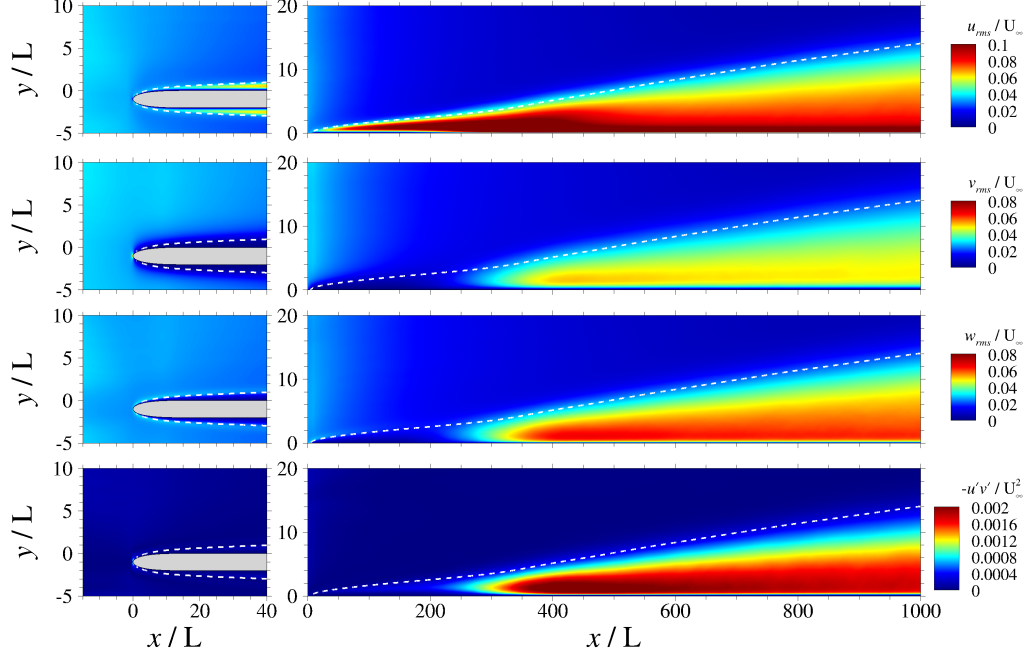


Figure 6: Contour plots the r.m.s. of (a) streamwise, (b) vertical and (c) spanwise velocity fluctuations. (d) Reynolds shear stress,  $-\overline{u'v'}$ . All quantities are normalized by  $U_\infty$ . The dashed line marks the iso-contour  $u = 0.99U_\infty$ .

### Simulation parameters

- Inflow free stream velocity:  $U_\infty = 1$  reference velocity scale
- Half thickness of the plate:  $L = 1$  reference lengths scale
- Viscosity:  $\nu = 1.25 \times 10^{-3}$
- Simulation domain Length:  $L_\xi \times L_\eta \times L_z = (1099 \times 40 \times 240) L$  in curvilinear coordinates
- Plate length:  $L_x = 1050L$
- Simulation grid:  $N_\xi \times N_\eta \times N_z = 4097 \times 257 \times 2049$
- Simulation time step:  $\Delta t = 0.005L/U_\infty$
- Isotropic turbulence at the curved simulation inlet: 3.5%
- Database domain:  $x \times y \times z = [30.2185, 1000.065]L \times [0.0036, 26.4880]L \times [0, 240]L$
- Database domain Length:  $L_x \times L_y \times L_z = (969.8465 \times 26.4844 \times 240)L$
- Database grid:  $N_x \times N_y \times N_z = 3320 \times 224 \times 2048$
- Database time step:  $\Delta t = 0.25L/U_\infty$
- Isotropic turbulence at the database inlet ( $x/L = 30.2185$ ): 2.86%
- Time stored:  $t \in [0, 1175.0]L/U_\infty$

## Flow statistics within the JHTDB sub-domain, averaged in span and $t \in [0, 1175.0]$

- Boundary layer thickness:  $\delta_{99} = 0.9648 - 15.0433L$
- Momentum thickness:  $\theta = 0.1318 - 1.8775L$
- Reynolds number based on boundary-layer thickness:  $Re_\delta \equiv U_\infty \delta_{99} / \nu = 772 - 12035$
- Reynolds number based on momentum thickness:  $Re_\theta \equiv U_\infty \theta / \nu = 105.5 - 1502.0$

*Note 1:* In the JHTDB analysis tools for this dataset, only the 4th-order Lagrange Polynomial interpolation scheme and the 4th-order finite differencing scheme (*Lag4*, *FD4NoInt* and *FD4Lag4*) are implemented. Higher order schemes are not provided since the DNS was performed using second-order methods.

*Note 2:* The divergence-free condition in the simulation is enforced based on a Helmholtz equation. The JHTDB analysis tools for gradients are based on 4th-order finite differencing. Therefore, when evaluating the divergence using these spatially less localized derivative operators, a non-negligible error in the divergence is obtained, as expected.

*Note 3:* Since the grid is staggered, data at the wall are not stored in the database. However, the JHTDB provides values in the region  $y/L \in [0, 0.0036]$  for user's convenience. Specifically, *GetVelocity* and *GetPosition* will enforce  $u = v = w = 0$  at the wall ( $y = 0$ ) and use the zero-velocity condition to perform the interpolation in the region  $y \in [0, 0.0036]$ . Other *GetFunctions* (i.e. *GetPressure*, *GetVelocityGradient*, *GetPressureGradient*, *GetVelocityHessian*, *GetPressureHessian*, *GetVelocityLaplacian* and *GetInvariant*) will return extrapolated values using the 4th-order Lagrange Polynomial method and using only the data on the fluid grid points to perform interpolation/extrapolation.

## Acknowledgements

This work has been supported by the National Science Foundation (NSF, grants 1605404, CBET-1507469 and OCE-1633124). The computations were performed using the Extreme Science and Engineering Discovery Environment (XSEDE), which is supported by NSF (grant ACI-1053575).

## References

- LEE, J., JUNG, S. Y., SUNG, H. J. & ZAKI, T. A. 2013 Effect of wall heating on turbulent boundary layers with temperature-dependent viscosity. *Journal of Fluid Mechanics* **726**, 196–225.
- LEE, J., SUNG, H. J. & ZAKI, T. A. 2017 Signature of large-scale motions on turbulent/non-turbulent interface in boundary layers. *Journal of Fluid Mechanics* **819**, 165–187.
- LEE, J. & ZAKI, T. A. 2018 Detection algorithm for large-scale structures in turbulent/non-turbulent intermittent flow. *arXiv* .
- NOLAN, K. P. & ZAKI, T. A. 2013 Conditional sampling of transitional boundary layers in pressure gradients. *Journal of Fluid Mechanics* **728**, 306–339.
- ROACH, P. & BRIERLEY, D. 1992 The influence of a turbulent free-stream on zero pressure gradient transitional boundary layer development(prediction methods in cfd applications). *Numerical simulation of unsteady flows and transition to turbulence* pp. 319–347.

- ROSENFELD, M., KWAK, D. & VINOKUR, M. 1991 A fractional step solution method for the unsteady incompressible navier-stokes equations in generalized coordinate systems. *Journal of Computational Physics* **94** (1), 102–137.
- SCHLATTER, P., ÖRLÜ, R., LI, Q., BRETHOUWER, G., FRANSSON, J. H., JOHANSSON, A. V., ALFREDSSON, P. H. & HENNINGSON, D. S. 2009 Turbulent boundary layers up to  $Re_\theta = 2500$  studied through simulation and experiment. *Physics of fluids* **21** (5), 051702.
- WANG, L.-P., CHEN, S., BRASSEUR, J. G. & WYNGAARD, J. C. 1996 Examination of hypotheses in the Kolmogorov refined turbulence theory through high-resolution simulations. Part 1. Velocity field. *Journal of Fluid Mechanics* **309**, 113–156.
- ZAKI, T., WISSINK, J., RODI, W. & DURBIN, P. 2010 Direct numerical simulations of transition in a compressor cascade: the influence of free-stream turbulence. *Journal of Fluid Mechanics* **665**, 57–98.
- ZAKI, T. A. 2013 From streaks to spots and on to turbulence: exploring the dynamics of boundary layer transition. *Flow, turbulence and combustion* **3** (91), 451–473.